Kinetic Studies and Temperature-Induced Morphological Changes of Peptide Decorated Nano-Objects via Polymerization-Induced Self-Assembly

Belkacem Tarek Benkhaled, Hamza Chouirfa, Lubomir Vezenkov, Chaimaa Gomri, Arnaud Chaix, Gilles Subra, Vincent Ladmiral, Mona Semsarilar

Macromolecular Chemistry and Physics
www.mcp-journal.de

Kinetic Studies and Temperature-Induced Morphological Changes of Peptide Decorated Nano-Objects via Polymerization-Induced Self-Assembly

*Belkacem Tarek Benkhaled, Hamza Chouirfa, Lubomir Vezenkov, Chaimaa Gomri, Arnaud Chaix, Gilles Subra, Vincent Ladmiral, and Mona Semsarilar**

In the present work, combining polymerization-induced self-assembly (PISA) with self-assembling peptides (SAPs) peptide—polymer hybrid nanostructures are prepared, harnessing the advantages of PISA and the self-assembling driving force of SAPs. A tripeptide methacrylamide denoted as MAm-GFF, where MAm, G, and F stand for methacrylamide, glycine, and phenylalanine, is copolymerized with glycerol monomethacrylate (GMA) by reversible addition—fragmentation chain transfer polymerization (RAFT) in dimethylformamide to produce a P(GMA_{62}-*stat*-(MAm-$GFF)_7$) macromolecular chain transfer agent (macro-CTA). This peptide-containing macro-CTA is then successfully chain-extended with poly(2-hydroxypropyl methacrylate) (PHPMA) by aqueous dispersion PISA, forming P(GMA_{62}-*stat*-(MAm-$GFF)_7$)-*b*-$PHPMA_{27}$ self-assembled objects. The impacts of temperature and monomer conversion on the morphologies formed during the PISA process are investigated by analyzing samples withdrawn at different time during the polymerization of HPMA using transmission electron microscopy (TEM) and dynamic light scattering (DLS) at different temperatures (5–70 °C).

1. Introduction

Self-assembling peptides (SAPs) have been extensively studied for their ability to form nanoscale ordered structures. Among the 20 well-known amino acids, histidine (H),[1–3] tryptophan (W),[4–6] and phenylalanine (F)[4,7] are known to self-assemble forming a variety of morphologies such as fibers,[8,9] ribbons,[10,11] tapes,[12,13] tubes,[11] or rods.[14,15] Their self-assembly is driven by noncovalent interactions such as hydrogen bonding, $\pi-\pi$ stacking, van der Waals forces, and electrostatic interactions.[16] Thus, their organization could be triggered and finely regulated by different parameters such as ionic strength, pH, and temperature. Nano-objects based on SAP have also gained attention, especially for tissue engineering and drug delivery applications[17] because of their biocompatibility and ease of synthesis and modification to yield bioactivity.[18,19]

Polymers can also self-assemble into nano-objects and polymerization-induced self-assembly (PISA) offers efficient and reproducible ways of achieving this self-assembly.[20,21] PISA has been exploited as a facile and efficient route to produce various amphiphilic block copolymer nano-objects, whose self-assembly is governed predominantly by the interactions of the different blocks with the polymerization medium. In PISA the self-assembly occurs concomitantly during the formation of the block copolymer. A solvent-soluble polymer is chain extended with a solvent-insoluble polymer, generally using a reversible deactivation radical polymerization (RDRP) technique,[22–28] so that the self-assembly occurs as the polymerization progresses and the resulting morphologies depend on the volume fractions of the soluble and insoluble polymer segments. This simple synthetic method has gained momentum over the last decade for its ability to produce well-defined polymer nano-objects at high concentrations with high reproducibility. PISA has been demonstrated to work well under dispersion[29–31] or emulsion polymerization[32–34] conditions both in polar (water, alcohols, etc.)[35–38] and nonpolar solvents (alkanes, toluene, etc.).[39–41] Less conventional solvents such as ionic liquids[30] or supercritical CO_2[42–44] were also successfully used successfully in PISA protocols. PISA produces a

B. T. Benkhaled, H. Chouirfa, C. Gomri, A. Chaix, M. Semsarilar
Institut Européen des Membranes
IEM, Univ Montpellier, CNRS, ENSCM
Montpellier, France
E-mail: mona.semsarilar@umontpellier.fr

L. Vezenkov, G. Subra
Institut des Biomolécules Max Mousseron
IBMM, Univ Montpellier, CNRS, ENSCM
Montpellier, France

V. Ladmiral
Institut Charles Gerhardt Montpellier
ICGM, Univ Montpellier, CNRS, ENSCM
Montpellier, France

The ORCID identification number(s) for the author(s) of this article can be found under https://doi.org/10.1002/macp.202300178

DOI: 10.1002/macp.202300178

large variety of morphologies with controlled size and functionality, in particular spheres, worms, or vesicles when self-assembly is mainly or only governed by hydrophobic interactions. are the most common.[21,45–48]

Peptide–polymer hybrids are an important class of materials combining the specific characteristics of their peptide and polymer components. These structures can possess the biocompatibility and bioactivity of peptides and the robustness and functionality due to the polymer chains. Thus, such hybrid materials have been prepared by various approaches such as post-polymerization grafting, grafting-from, or grafting-through,[49–53] resulting in a wide variety of morphologies, functionalities, and potential applications. In our previous studies, we reported the first polypeptide–polymer nanoparticles synthesized via PISA.[54] These hybrid particles were composed of a hydrophilic trilysine-containing shell and a PHPMA hydrophobic core. The cationic oligo-Lysine was shown to confer antibacterial properties to the self-assembled structures.[54]

Exploring the combination of SAP and PISA should be sufficiently fruitful. The resulting block copolymer self-assemblies could be significantly influenced not only by physicochemical parameters such as the solubility and the hydrophobic/hydrophilic balance between the two components of the block copolymers but also by the specific self-recognition properties of the peptide moieties.

Recently, Dao et al.[7,55] investigated the synthesis and self-assembly of P(GMA_{65}-*stat*-(MAm-GFF)$_7$)-*b*-$PHPMA_{28}$ diblock. This polymer was prepared from a methacrylamide (MAm)-functionalized tripeptide monomer (MAm-Gly-Phe-Phe-NH_2, denoted MAm-GFF). MAm-GFF was statistically copolymerized with a hydrophilic monomer (glycerol monomethacrylate, GMA) by reversible addition–fragmentation chain-transfer (RAFT) polymerization to form the target SAP-containing macromolecular chain transfer agent (macro-CTA). This (MAm-GFF)-containing macro-CTA was chain-extended with poly (2-hydroxypropyl methacrylate) (PHPMA) via aqueous dispersion PISA.

This prior study demonstrated, for the first time, that the incorporation of only a handful of SAP units into a synthetic polymer strongly influences the shape and size of PISA-generated self-assembled structures.[7,56]

The structures and the evolution upon heating or cooling of the P(GMA_{65}-*stat*-(MAm-GFF)$_7$)-*b*-$PHPMA_{28}$ block polymer self-assembly were examined. At 70 °C, highly anisotropic fibers with 1–2 μm length and 50–100 nm width formed, whereas they changed to worm-like micelles (80–100 nm in length and 50 nm in width) at 20 °C. This morphological transition was fully reversible and is probably due to the local rearrangement of the peptide moieties. The thermosensitive properties of PHPMA at a lower temperature (4 °C)[57,58] were also observed as the rod-like structures observed at 70 °C turned into nanostructured spherical objects.

The present article aims to better understand the link between polymerization kinetics (instantaneous degree of polymerization) and the morphological behavior of these P(GMA_{65}-*stat*-(MAm-GFF)$_7$)-*b*-$PHPMA_{28}$ diblock polymer nanostructures. Here, a P(GMA_{62}-*stat*-(MAm-GFF)$_7$)-*b*-$PHPMA_{27}$ block copolymer was synthesized via PISA and the evolution of the morphologies occurring in the course of the PISA (i.e., during the aqueous RAFT dispersion polymerization of HPMA) was examined. In other words, this manuscript explores the influence of the balance between the stabilizing GFF-containing statistical copolymer (P(GMA_{65}-*stat*-(MAm-GFF)$_7$) and the thermosensitive PHPMA block on the self-assembly process. The nanostructures obtained at different HPMA conversions were characterized at different temperatures.

The synthetic approach in this work is illustrated in **Scheme 1** and follows our previously reported methods.[7,55] Scattering and imaging techniques were used to characterize the resulting nano-objects.

2. Experimental Section

2.1. Materials

2-Hydroxypropyl methacrylate (HPMA, 97% purity) and 4,4'-azobis(4-cyanopentanoic acid) (ACVA, 98% purity) were purchased from Sigma-Aldrich. Glycerol monomethacrylate (GMA, purity 97%) was purchased from Apollo Scientific (UK). The NMR deuterated solvent (DMSO-d_6) was also purchased from Sigma-Aldrich. The RAFT agent 4-cyano-4-(2-phenylethane-sulfanyl thiocarbonyl)-sulfanylpentanoic acid (PETTC, 98% purity) was prepared as previously described.[37] The methacrylamide-functionalized peptide monomer (MAm-GFF) was prepared as described in a previous paper using solid phase peptide synthesis.[7] All reagents were used as received.

2.2. RAFT Copolymerization of GMA and MAm-GFF

The general procedure for the synthesis of the P(GMA_{62}-*co*-MAm-GFF_7) macro-CTA was described previously (Scheme 1).[7] The molar ratios were defined as such [GMA]:[MAm-GFF]:[PETTC]:[ACVA] [66]:[9]:[1]:[0.1]. A round bottom flask equipped with a stirrer bar was charged with GMA (0.71 g, 4.3 mmol), MAm-GFF (0.26 g, 0.58 mmol), PETTC RAFT agent (22.4 mg, 0.065 mmol) ACVA initiator (2.0 mg, 0.007 mmol) and DMF (2.62 mL). The flask was sealed and placed in an ice-cold bath while the solution was degassed by bubbling nitrogen for 30 min. Then, the flask was immersed in a pre-heated oil bath at 70 °C for 24 h under magnetic agitation. After 24 h, an aliquot was taken to determine the conversion in ^{1}H NMR (GMA conversion = 93%, MAm-GFF conversion = 72%). The solution was precipitated once in cold chloroform to remove unreacted monomer, and then the yellow precipitate was filtered and dried under vacuum at 40 °C overnight. The polymer was analyzed in dimethylacetamide (DMAC) GPC (M_n = 34.8 kg mol^{-1}; $Đ$ = 1.15) and by ^{1}H NMR spectroscopy.

2.3. PISA via RAFT Aqueous Dispersion Polymerization

PISA protocol was performed via RAFT aqueous dispersion polymerization of HPMA with P(GMA_{62}-*stat*-(MAm-GFF)$_7$) macro-CTA as described below (Scheme 1). The molar ratios of reactant used were [HPMA]:[P(GMA_{62}-*stat*-MAm-GFF_7)]:[ACVA] = [27]:[1]:[0.2]. The purified P(GMA_{62}-*stat*-(MAm-GFF)$_7$) macroCTA (201 mg, 0.015 mmol), HPMA (60.0 mg,

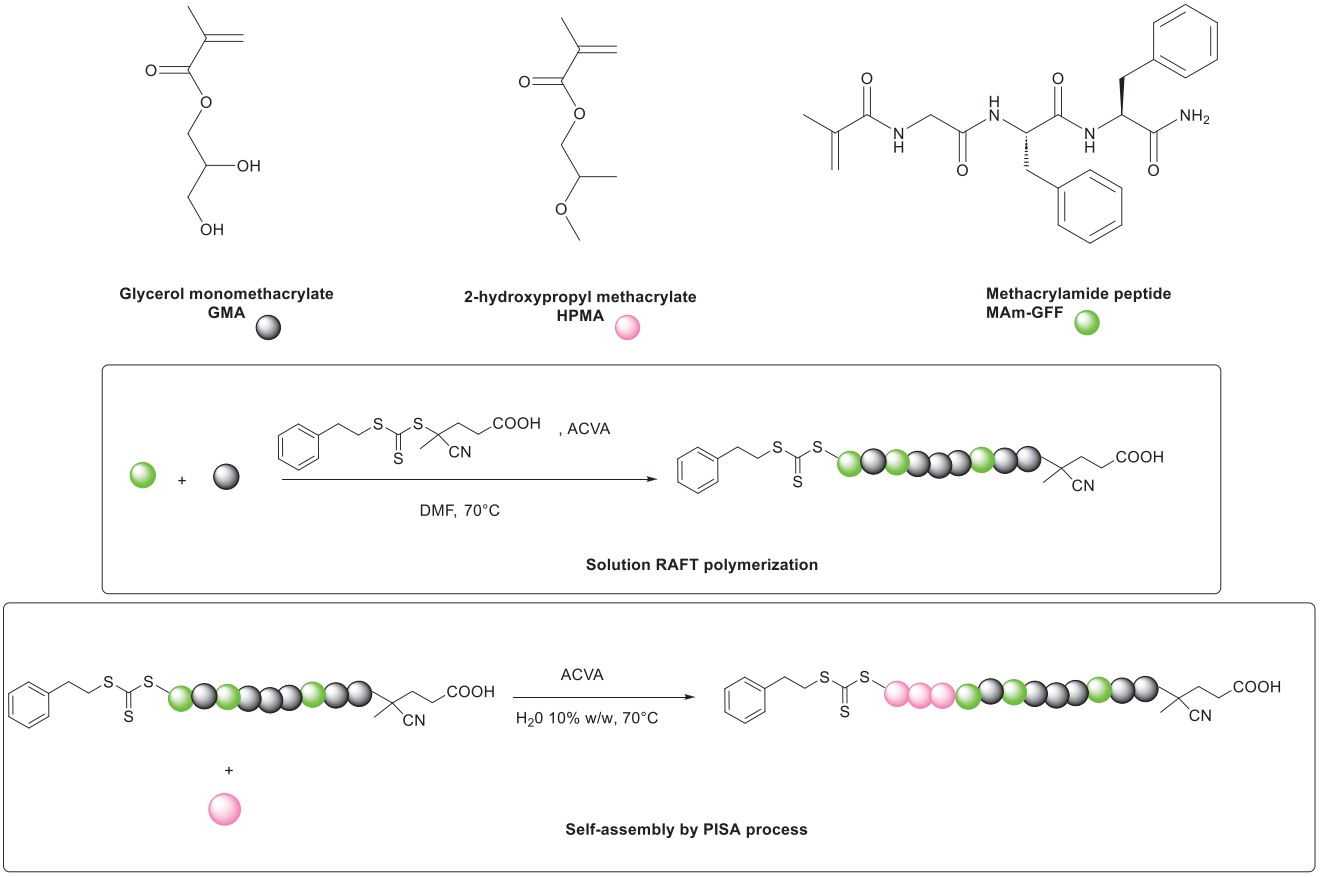

Scheme 1. Synthesis of the P(GMA$_{62}$-*stat*-(MAm-GFF)$_7$) macro-CTA using RAFT and of P(GMA$_{62}$-*stat*-(MAm-GFF)$_7$)-*b*-PHPMA$_n$ block copolymers under RAFT controlled aqueous dispersion polymerization at 70 °C and 10 w/w%.

0.406 mmol) and ACVA initiator (1.0 mg, 0.0035 mmol) were weighed into a 10-mL glass vial containing a stirrer bar. 2.38 mL MilliQ water was then added to get a reaction solution at 10% w/w. The vial was sealed, placed in an ice bath, degassed for 30 min, and then put into an oil bath previously thermostated at 70 °C using a stirring hotplate. After 24 h, the reaction vial was opened to air, cooled down to ambient temperature and aliquots were taken for ^{1}H NMR (GMA conversion = 99%), GPC (M_n = 42.7 kg mol^{-1}; $Đ$ = 1.2), TEM and DLS analyses.

2.3.1. Proton Nuclear Magnetic Resonance Spectroscopy (^{1}H NMR)

^{1}H NMR spectra were recorded on a 400 MHz Bruker Avance-400 spectrometer. The analyses were performed in DMSO-d$_6$.

2.3.2. Gel Permeation Chromatography (GPC)

Polymer molar mass distributions were analyzed using a Varian PL-50 GPC system fitted with 2 PolarGel M 300 × 7.5 columns thermostated at 50 °C. The mobile phase was DMAc containing 0.1% w/w LiCl at a flow rate of 0.8 mL min^{-1}. The calibration was achieved with near-monodisperse poly(methyl methacrylate) (PMMA) standards ranging from 550 to 1 500 000 g mol^{-1} (EasiVial-Agilent).

2.3.3. Dynamic Light Scattering (DLS)

The hydrodynamic radii were analyzed by dynamic light scattering at 90° using an Anton Paar Litesizer TM 500. Samples were prepared at 0.1% w/w by diluting the PISA suspension 100-fold with MilliQ water. Experiments were performed at 10 °C intervals from 10 to 70 °C, with 1 min being allowed for thermal equilibrium before each measurement.

2.3.4. Transmission Electronic Microscopy (TEM)

TEM images were acquired using either a JEOL 1200 EXII—120 kV or a JEOL 1400 P+—120 kV. 10 µL of diluted PISA suspension (0.1% w/w) was deposited onto the grid for 30 s and then blotted with filter paper to remove excess solution. Then, the sample-loaded grid was stained with 7 µL of 1% ammonium molybdate solution for 15 s before this solution was removed with filter paper. The grid was allowed to dry during 5 min in a fume hood. For the study at 70 °C, 10% w/w PISA suspension was incubated at the desired temperature for 1 h and diluted to 0.1% w/w with Milli-Q water at the same temperature. Samples were quickly loaded onto the grid using the protocol described above, but in these cases, the grids were prepared and kept in an oven chamber set at 70 °C.

Table 1. HPMA conversion, theoretical and experimental number-average molar mass, and dispersity of the PHPMA$_{27}$-*b*-P(GMA$_{62}$-*stat*-(MAm-GFF$_7$)).

Polymer	Conv.[a] [%]	$M_{n,th}$[b] [kg mol^{-1}]	$M_{n,GPC}$[c] [kg mol^{-1}]	$Đ$
P(GMA$_{62}$-*stat*-(MAm-GFF$_7$) (macroCTA)	93[d]/72[e]	13.3	34.8	1.15
P(GMA$_{62}$-*stat*-(MAm-GFF$_7$))-*b*-PHPMA$_{27}$	>99	16.6	42.7	1.19

[a] Determined using Equation (2); [b] As determined according to Equation (1); [c] Determined by size-exclusion chromatography; [d] Conversion of GMA. [e] Conversion of MAm-GFF.

2.3.5. Calculation of the $M_{n,th}$

The theoretical number-average molar masses ($M_{n,th}$) were calculated using the following equation (Equation (1)).[45]

$$M_{n,th} = \frac{[M]_0 \times pM_M}{[CTA]_0} + M_{CTA} \quad (1)$$

where $[M]_0$ and $[CTA]_0$ are the initial concentrations (in mol L^{-1}) of the monomer and the chain transfer agent. p is the monomer conversion as determined by ^{1}H NMR. M_M and M_{CTA} are the molar masses (in g mol^{-1}) of the monomer and the chain transfer agent respectively.

2.3.6. Calculation of HPMA Conversion

The HPMA conversion (p) was calculated using Equation (2)

$$p = \frac{\int_{6.1,tf}}{\int_{6.1,t0}} * 100 \quad (2)$$

where $\int_{6.1,t0}$ and $\int_{6.1,tf}$ are the respective integration at $t = t_0$ and $t = t_f$ respectively, by taking the protons of the phenylalanine (FF, 7.1–7.3 ppm) as reference.

3. Results and Discussions

3.1. RAFT Copolymerization of GMA and MAm-GFF

The synthesis of the macroCTA was performed according to our previous publication.[7,55] Briefly, the polymerization between the GMA and the MAm-GFF was performed at 70 °C for 24 h using ACVA as initiator and PETTC RAFT agent in DMF. ^{1}H NMR analysis showed conversions of 93% and 72% for GMA and MAm-GFF, respectively; resulting in a P(GMA$_{62}$-*stat*-MAm-GFF$_7$) copolymer with a calculated M_n = 13.3 kg mol^{-1} (**Table 1**). The polymerization was as expected well controlled as the GPC analysis in DMAc, revealed a M_n of 34.8 kg mol^{-1} and dispersity ($Đ$) of 1.15.

3.2. P(GMA$_{62}$-*stat*-(MAm-GFF)$_7$-*b*-PHPMA$_{27}$ via PISA Polymerization

The second block was synthesized in water (10% w/w) using the (P(GMA$_{62}$-*stat*-MAm-GFF)$_7$) macro-CTA synthesized in the previous step. As shown in **Figure 1**, polymerization of HPMA in water was very fast reaching 90% conversion in 40 min. After 150 min the HPMA conversion was 99% (calculated from ^{1}H NMR data using Equation (2)). Similar to other aqueous PISA in dispersion, the kinetics profile showed three polymerization regimes: a slow rate of polymerization corresponding to the solution polymerization of HPMA, a fast polymerization rate after the formation of the micelles that act as a nano-reactor providing a higher local concentration of HPMA; and a third slower rate of polymerization when the HPMA concentration has decreased (conversion >90%).[45,59]

Analysis of the kinetic samples taken at different time intervals by GPC showed that the molar mass of the forming diblock copolymers increased steadily with the increasing conversion of HPMA. The dispersity of this diblock copolymers remained between 1.12 and 1.19 (**Figure 2**), indicating a good controlled/living character.[60] The GPC traces of the copolymers (**Figure 3**), were monomodal, confirming the good chain-end

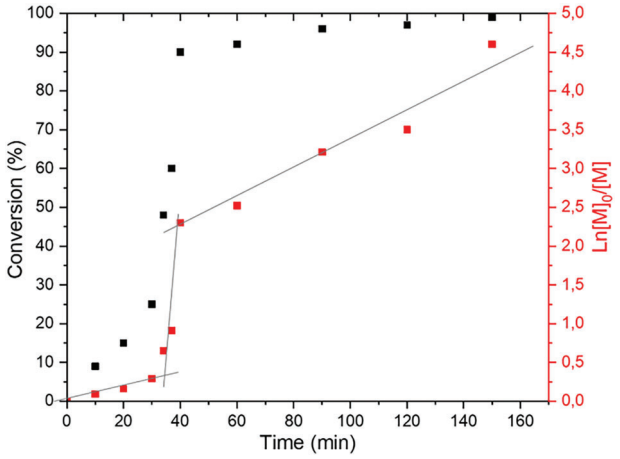

Figure 1. Evolution of the HPMA conversion versus time calculated from ^{1}H NMR (DMSO-d$_6$) and first kinetic plot of the HPMA polymerization (with target DP of 27).

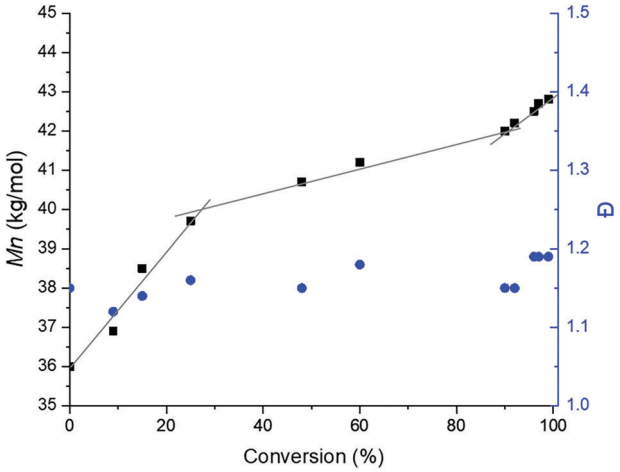

Figure 2. Evolution of the number-average molar mass and dispersity versus conversion for P(GMA$_{62}$-*stat*-MAm-GFF)$_7$-*b*-PHPMA$_{27}$ synthesized in water at 10% w/w at 70 °C.

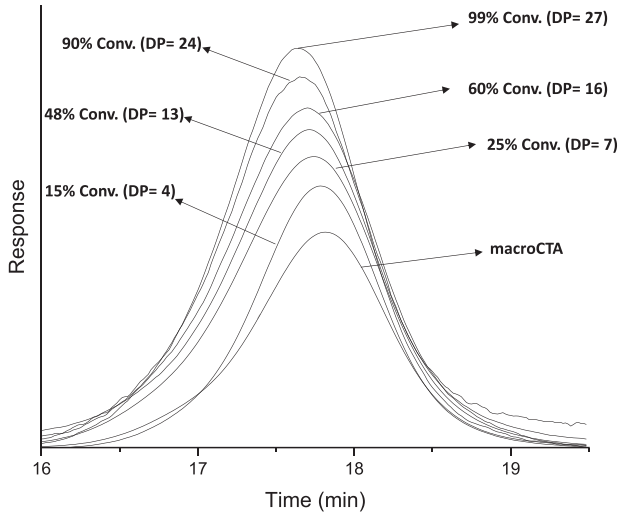

Figure 3. DMAc GPC traces (refractive index detector) for the P(GMA62-stat-(MAm-GFF)7) macro-CTA and the diblock copolymer P(GMA62-*stat*-(MAm-GFF)7)-*b*-PHPMA$_n$ at different polymerization times (with target DP of 27). The polymerization was performed under RAFT aqueous dispersion polymerization at 10% w/w at 70 °C.

fidelity of the macro-CTA as well as the controlled nature of the polymerization.

3.3. Temperature and Its Effect on Particle Morphology

DLS and TEM analyses were performed on samples withdrawn at various HPMA polymerization times to investigate the evolution of the (PGMA$_{62}$-*stat*-MAm-GFF$_7$)-*b*-PHPMA$_n$ block copolymer morphology (dispersed in Milli-Q water at 0.1% w/w, stirred gently overnight). TEM analysis of the 3 samples corresponding to $n = 13$, 24 and 25 (in (PGMA$_{62}$-*stat*-MAm-GFF$_7$)-*b*-PHPMA$_n$) (**Figure 4**) showed that at room temperature (≈20 °C) the PHPMA block does not have any significant impact on the morphology. The fibers formed by the macro-CTA were still present in all samples. As shown in our previous work,[7] the second block with maximum DP of 27 is not hydrophobic enough to trigger the formation of other morphologies at room temperature. The self-assembly was governed by the GFF moieties of the first block P(GMA$_{62}$-*stat*-MAm-GFF$_7$) thanks to the weak molecular interactions (electrostatic forces, hydrophobic interactions, π–π stacking and hydrogen bonding).

DLS analysis of kinetic samples showed different particle hydrodynamic diameters depending on the temperature (**Figure 5**). At the beginning of the polymerization the diameter of the fiber bundles formed by the macro-CTA was between 100 nm and 1 µm when temperature was increased from 10 to 70 °C. After 20 min of polymerization when the DP of the HPMA was about 4, the size of the self-assemblies was reduced to 100 nm over the same temperature range. As the DP was increased, the nano-object size was reduced. After one hour of polymerization (DP of 25), the hydrodynamic diameter of the objects stayed around 5–10 nm and did not vary on heating from 10 to 50 °C. However, at 60 and 70 °C the diameter increased to 100 nm (10–20 times bigger). At 90 min and PHPMA DP of 26, the size of the objects was 5–10 nm at 10 and 20 °C but increased to 100 nm above 30 °C. It is clear that increasing the length of the PHPMA block has a considerable effect on the thermoresponsivity of the assembled structures. Such PHPMA behavior has been previously described by Armes and co-workers previously.[46,57,58,61]

The representative TEM images at room temperature and 70 °C confirmed the effect of temperature on the morphology (**Figure 6**). The fibers formed by the SAP moieties disappeared when the temperature was increased as demonstrated in our previous work,[7,55] as well as by Huang.[18] At room temperature the

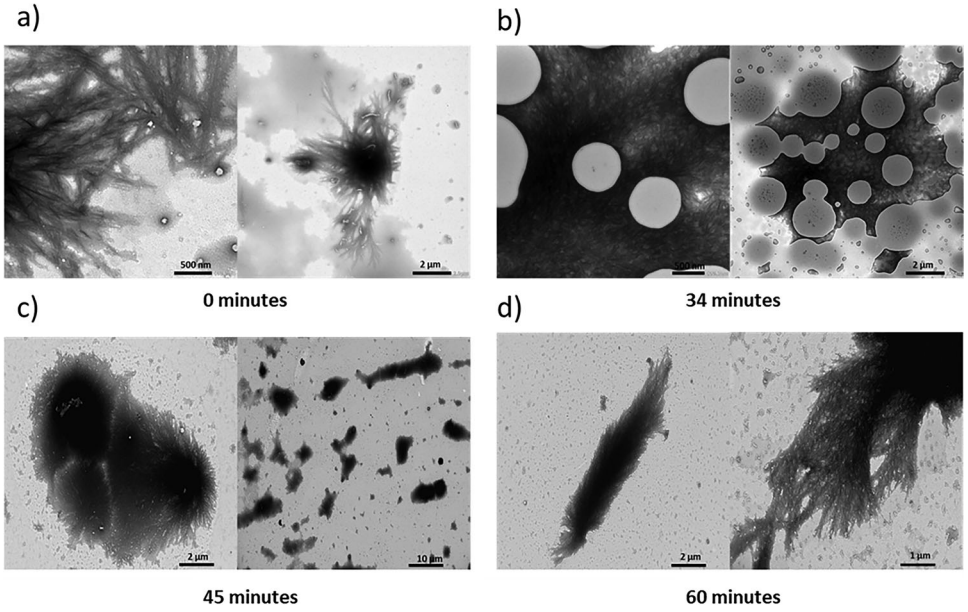

Figure 4. Representative TEM images of P(GMA$_{62}$-*stat*-Mam-GFF$_7$)-*b*-PHPMA$_n$ diblock copolymers prepared by PISA in water at different polymerization times a) $t = 0$; DP$_{HPMA} = 0$, b) $t = 34$ min; $n = 13$, c) $t = 45$ min; $n = 24$, and d) $t = 60$ min; $n = 25$ at room temperature.

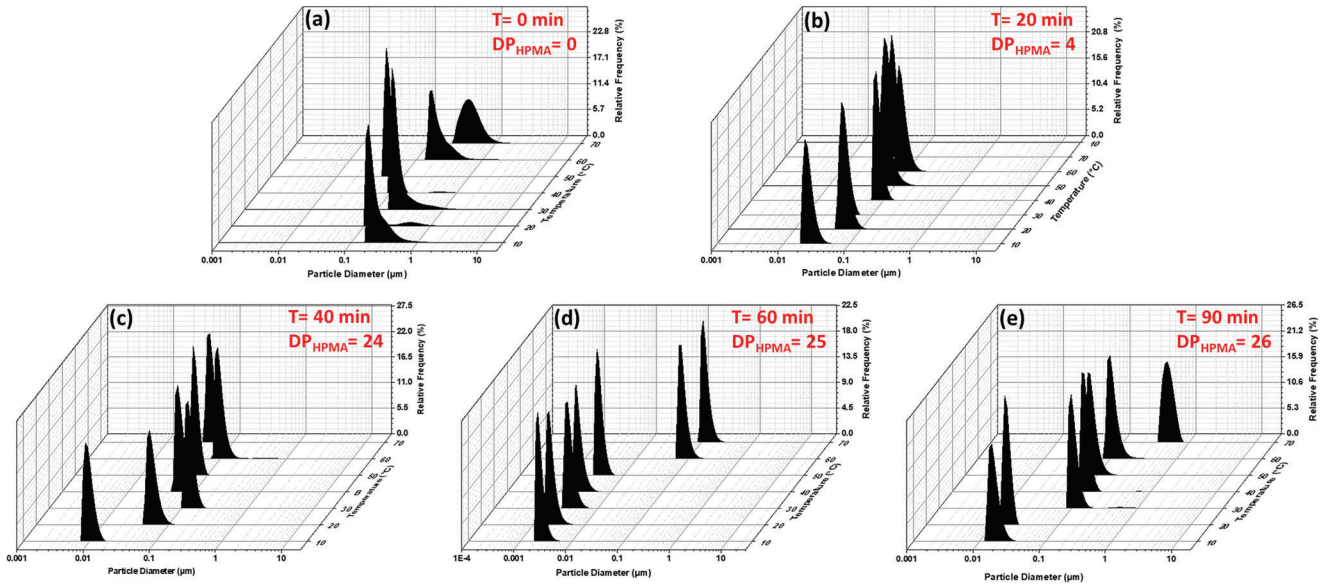

Figure 5. Evolution of the particle diameter of (PGMA$_{62}$-*stat*-Mam-GFF$_7$)- *b*-PHPMA$_n$ diblock copolymer at 0.1% w/w in water at a different temperature according to different polymerization kinetic points after a) $t = 0$; DP$_{HPMA}$ = 0, b) $t = 20$ min; $n = 4$, c) $t = 40$ min; $n = 24$, d) $t = 60$ min; $n = 25$, and e) 90; $n = 26$.

self-assembly is driven by the intermolecular interactions (e.g., π–π interaction) of the SAP, while at higher temperature (>60 °C) the fibers disassemble due to the temperature-triggered breakdown of these weak interactions. Moreover, disassembly at 70 °C and re-assembly at room temperature was fully reversible. When changing the temperature, there are two forces in action; SAP interactions that are weakened as temperature increases and the slightly higher partial degree of hydration of the PHPMA chains at sub-ambient temperatures (lower than 20 °C). Heating does not only increase the mobility of the chains but it also weakens the hydrogen bonds and π–π interaction.[19,62,63] At high temperature, when the interactions between GFF moieties are sufficiently reduced or completely negated, the P(GMA$_{62}$-*stat*-(MAm-GFF)$_7$)-*b*-PHPMA$_{27}$ morphology is governed only by the partial degree of hydration of the PHPMA block. At lower temperatures, the self-assembly is mainly influenced by the SAP interaction as the hydrophilicity of the PHPMA chains is increased. In the absence of SAP the self-assemblies would have fall apart as the PHPMA chains would become slightly more hydrated at low temperatures as reported by Armes and co-workers. They demonstrated that the PGMA-*b*-PHPMA block copolymer particles exhibit thermo-responsive behavior with reversible morphology transition from worms to spheres upon cooling to 4 °C.[57,58,61] Hence, the self-assembly process of the SAP containing block copolymer is not

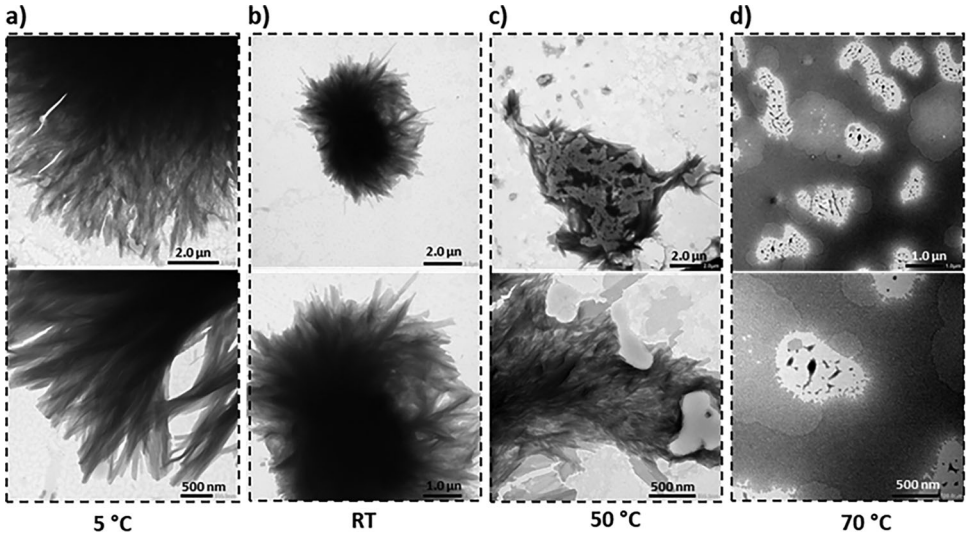

Figure 6. Representative TEM images of diblock copolymers (PGMA$_{62}$-*stat*-MAm-GFF$_7$)-*b*-PHPMA$_{27}$ prepared by PISA in water after 2 h of polymerization, at different temperatures: a) 5 °C, b) room temperature, c) 50 °C, and d) 70 °C. TEM samples concentration = 0.1% w/w.

only driven by the specific peptide interactions but also by the delicate balance between hydrophobicity and hydrophilicity of the entire system.

4. Conclusion

This study showed in detail the effect of the balance between the first block containing peptide ($PGMA_{62}$-*stat*-MAm-GFF_7) and the second PHPMA block on the morphology and the size of the ($PGMA_{62}$-*stat*-Mam-GFF_7)-*b*-$PHPMA_n$ nano-objects. Also, the impact of the temperature on the morphologies at different DPs of PHPMA has been examined. First, A $PGMA_{62}$-*stat*-MAm-GFF_7 macro-CTA able to self-assemble due to the weak peptide interactions, namely π–π interactions and hydrogen bonding of GFF moieties was prepared by RAFT polymerization. Then, the PISA process at 10% w/w in water allowed the synthesis of ($PGMA_{62}$-*stat*-Mam-GFF_7)-*b*-$HPMA_{27}$ diblock copolymer. This article supplements our previous study[7] by demonstrating that at room temperature the self-assembly is mainly driven by peptide interaction of the SAP moieties, where fibrous nano-objects were observed in TEM images. It was also noticed that when the temperature was raised, the fibrous structures formed at 5 °C and room temperature, started to fall apart, due to the weakening of the hydrogen bonding and π–π interaction of the SAP moieties, as well as the change in the solubility of the PHPMA block at higher temperatures. Besides the TEM images, the DLS measurements at different temperatures also showed that, the size of the objects increases from 10 to 100 nm upon increasing the temperature. Varying the temperature induced a remarkable reversible morphological change in the fiber-like structures formed by P(GMA_{62}-*stat*-(MAm-$GFF)_7$)-*b*-$PHPMA_n$ as detected by both DLS and TEM. This study highlights the essential role of the peptide interactions and the effect of temperature in the process of self-assembly. These results along with the structural diversity of the polypeptides and the numerous different possibilities in their sequence could pave the way for the design of a wide range of self-assembled objects with potential biomedical applications such as asymmetric drug delivery systems or original scaffolds for tissue engineering.

Acknowledgements

This work was funded by project PEPPISA (ANR-19-CE06-0011-01). The authors would also like to thank the C3M team from ICGM (University of Montpellier) for the GPC characterization.

Conflict of Interest

The authors declare no conflict of interest.

Author Contributions

B.T.B. and H.C. contributed equally to this work. The authors who are the undersigned declare that this manuscript is original, has not been published before and is not currently being considered for publication elsewhere. We confirm that the manuscript has been read and approved by all named authors and that there are no other persons who satisfied the criteria for authorship but are not listed. The authors further confirm that the order of authors listed in the manuscript has been approved by all the authors. They understand that the Corresponding Author is the sole contact for the Editorial process. She is responsible for communicating with the other authors about progress, submissions of revisions, and final approval of proofs.

Conceptualization: H.C., C.G., B.T.B., A.C., L.V., G.S., V.L., M.S. Methodology: H.C., C.G., B.T.B., A.C., L.V., M.S. Validation: H.C., C.G., B.T.B., A.C., L.V., M.S. Formal analysis: H.C., C.G., B.T.B., A.C., M.S. Investigation: H.C., C.G., B.T.B., A.C. Resources: G.S., L.V., V.L., M.S. Writing–Original draft: H.C., B.T.B., M.S. Writing–Review and editing: H.C., C.G., B.T.B., A.C., G.S., L.V., V.L., M.S. Visualization: H.C., C.G., B.T.B., A.C., L.V., M.S. Supervision: L.V., V.L., M.S. Project administration: M.S. Funding acquisition: M.S.

Data Availability Statement

The data that support the findings of this study are available from the corresponding author upon reasonable request.

Keywords

colloidal particles, peptide-polymer conjugates, PISA, SAP, self-assembly

Received: June 7, 2023
Revised: August 1, 2023
Published online:

[1] M. Hatip Koc, G. Cinar Ciftci, S. Baday, V. Castelletto, I. W. Hamley, M. O. Guler, *Langmuir* **2017**, *33*, 7947.
[2] D. Madrigal-Trejo, P. S. Villanueva-Barragán, R. Zamudio-Ramírez, K. E. Cervantes-de la Cruz, I. Mejía-Luna, E. Chacón-Baca, A. Negrón-Mendoza, S. Ramos-Bernal, A. Heredia-Barbero, *Origins Life Evol. Biospheres* **2021**, *51*, 117.
[3] E. R. L. Brisson, J. C. Griffith, A. Bhaskaran, G. V. Franks, L. A. Connal, *J. Polym. Sci., Part A: Polym. Chem.* **2019**, *57*, 1964.
[4] S. Bera, B. Xue, P. Rehak, G. Jacoby, W. Ji, L. J. W. Shimon, R. Beck, P. Král, Y. Cao, E. Gazit, *ACS Nano* **2020**, *14*, 1694.
[5] C. Diaferia, N. Balasco, T. Sibillano, C. Giannini, L. Vitagliano, G. Morelli, A. Accardo, *ChemPhysChem* **2018**, *19*, 1635.
[6] D. G. Babar, S. Sarkar, *Appl. Nanosci.* **2017**, *7*, 101.
[7] T. P. T. Dao, L. Vezenkov, G. Subra, M. Amblard, M. In, J. F. Le Meins, F. Aubrit, M. A. Moradi, V. Ladmiral, M. Semsarilar, *Macromolecules* **2020**, *53*, 7034.
[8] S. Debnath, S. Roy, R. V Ulijn, *J. Am. Chem. Soc.* **2013**, *135*, 16789.
[9] G. Cinar, I. Orujalipoor, C.-J. Su, U.-S. Jeng, S. Ide, M. O. Guler, *Langmuir* **2016**, *32*, 6506.
[10] A. M. Aberle, H. K. Reddy, N. V. Heeb, K. P. Nambiar, *Biochem. Biophys. Res. Commun.* **1994**, *200*, 102.
[11] A. Rüter, S. Kuczera, J. Stenhammar, T. Zinn, T. Narayanan, U. Olsson, *Phys. Chem. Chem. Phys.* **2020**, *22*, 18320.
[12] S. Maude, D. E. Miles, S. H. Felton, J. Ingram, L. M. Carrick, R. K. Wilcox, E. Ingham, A. Aggeli, *Soft Matter* **2011**, *7*, 8085.
[13] R. P. W. Davies, A. Aggeli, *J. Pept. Sci.* **2011**, *17*, 107.
[14] A. Aggeli, I. A. Nyrkova, M. Bell, R. Harding, L. Carrick, T. C. B. McLeish, A. N. Semenov, N. Boden, *Proc. Natl. Acad. Sci. USA* **2001**, *98*, 11857.
[15] N. J. Sinha, D. Wu, C. J. Kloxin, J. G. Saven, G. V Jensen, D. J. Pochan, *Soft Matter* **2019**, *15*, 9858.
[16] J. Kim, T. H. Han, Y.-I. Kim, J. S. Park, J. Choi, D. G. Churchill, S. O. Kim, H. Ihee, *Adv. Mater.* **2010**, *22*, 583.
[17] G. Moad, E. Rizzardo, S. H. Thang, G. Moad, E. Rizzardo, S. H. Thang, *Aust. J. Chem.* **2005**, *58*, 379.

[18] R. Huang, Y. Wang, W. Qi, R. Su, Z. He, *Nanoscale Res. Lett.* **2014**, *9*, 1.
[19] J. Wang, K. Liu, R. Xing, X. Yan, *Chem. Soc. Rev.* **2016**, *45*, 5589.
[20] C. Liu, C.-Y. Hong, C.-Y. Pan, *Polym. Chem.* **2020**, *11*, 3673.
[21] N. J. W. Penfold, J. Yeow, C. Boyer, S. P. Armes, *ACS Macro Lett.* **2019**, *8*, 1029.
[22] M. Semsarilar, V. Abetz, *Macromol. Chem. Phys.* **2021**, *222*, 2000311.
[23] F. D'Agosto, J. Rieger, M. Lansalot, *Angew. Chem., Int. Ed.* **2020**, *59*, 8368.
[24] E. Guégain, C. Zhu, E. Giovanardi, J. Nicolas, *Macromolecules* **2019**, *52*, 3612.
[25] L. P. D. Ratcliffe, A. J. Ryan, S. P. Armes, *Macromolecules* **2013**, *46*, 769.
[26] S. Varlas, J. C. Foster, R. K. O'Reilly, *Chem. Commun.* **2019**, *55*, 9066.
[27] J. Wang, Z. Wu, G. Wang, K. Matyjaszewski, *Macromol. Rapid Commun.* **2019**, *40*, 1800332.
[28] A. Darabi, P. G. Jessop, M. F. Cunningham, *Macromolecules* **2015**, *48*, 1952.
[29] M. Semsarilar, V. Ladmiral, A. Blanazs, S. P. Armes, *Langmuir* **2012**, *28*, 914.
[30] A. Blanazs, A. J. Ryan, S. P. Armes, *Macromolecules* **2012**, *45*, 5099.
[31] M. Semsarilar, V. Ladmiral, A. Blanazs, S. P. Armes, *Langmuir* **2013**, *29*, 7416.
[32] S. Boissé, J. Rieger, K. Belal, A. Di-Cicco, P. Beaunier, M.-H. Li, B. Charleux, *Chem. Commun.* **2010**, *46*, 1950.
[33] I. Chaduc, A. Crepet, O. Boyron, B. Charleux, F. D'Agosto, M. Lansalot, *Macromolecules* **2013**, *46*, 6013.
[34] I. Chaduc, W. Zhang, J. Rieger, M. Lansalot, F. D'Agosto, B. Charleux, *Macromol. Rapid Commun.* **2011**, *32*, 1270.
[35] M. J. Derry, L. A. Fielding, S. P. Armes, *Prog. Polym. Sci.* **2016**, *52*, 1.
[36] M. Semsarilar, V. Ladmiral, A. Blanazs, S. P. Armes, *Polym. Chem.* **2014**, *5*, 3466.
[37] M. Semsarilar, N. J. W. Penfold, E. R. Jones, S. P. Armes, *Polym. Chem.* **2015**, *6*, 1751.
[38] W. Zhao, G. Gody, S. Dong, P. B. Zetterlund, S. Perrier, *Polym. Chem.* **2014**, *5*, 6990.
[39] L. A. Fielding, M. J. Derry, V. Ladmiral, J. Rosselgong, A. M. Rodrigues, L. P. D. Ratcliffe, S. Sugihara, S. P. Armes, *Chem. Sci.* **2013**, *4*, 2081.
[40] M. J. Derry, L. A. Fielding, S. P. Armes, *Polym. Chem.* **2015**, *6*, 3054.
[41] A. P. Lopez-Oliva, N. J. Warren, A. Rajkumar, O. O. Mykhaylyk, M. J. Derry, K. E. B. Doncom, M. J. Rymaruk, S. P. Armes, *Macromolecules* **2015**, *48*, 3547.
[42] D. Zhou, R. P. Kuchel, S. Dong, F. P. Lucien, S. Perrier, P. B. Zetterlund, *Macromol. Rapid Commun.* **2019**, *40*, 1800335.
[43] S. Dong, W. Zhao, F. P. Lucien, S. Perrier, P. B. Zetterlund, *Polym. Chem.* **2015**, *6*, 2249.
[44] A. Xu, Q. Lu, Z. Huo, J. Ma, B. Geng, U. Azhar, L. Zhang, S. Zhang, *RSC Adv.* **2017**, *7*, 51612.
[45] A. Blanazs, J. Madsen, G. Battaglia, A. J. Ryan, S. P. Armes, *J. Am. Chem. Soc.* **2011**, *133*, 16581.
[46] N. J. Warren, S. P. Armes, *J. Am. Chem. Soc.* **2014**, *136*, 10174.
[47] S. Sugihara, A. Blanazs, S. P. Armes, A. J. Ryan, A. L. Lewis, *J. Am. Chem. Soc.* **2011**, *133*, 15707.
[48] D. Le, D. Keller, G. Delaittre, D. Le, D. Keller, G. Delaittre, *Macromol. Rapid Commun.* **2019**, *40*, 1800551.
[49] I. Cobo, M. Li, B. S. Sumerlin, S. Perrier, *Nat. Mater.* **2014**, *14*, 143.
[50] B. S. Sumerlin, *ACS Macro Lett.* **2012**, *1*, 141.
[51] N. Vanparijs, R. De Coen, D. Laplace, B. Louage, S. Maji, L. Lybaert, R. Hoogenboom, B. G. De Geest, *Chem. Commun.* **2015**, *51*, 13972.
[52] A. El Jundi, M. Mayor, E. Folgado, C. Gomri, B. T. Benkhaled, A. Chaix, P. Verdie, B. Nottelet, M. Semsarilar, *Eur. Polym. J.* **2022**, *176*, 111386.
[53] J. Martin, A. Desfoux, J. Martinez, M. Amblard, A. Mehdi, L. Vezenkov, G. Subra, *Prog. Polym. Sci.* **2021**, *115*, 101377.
[54] L. Luppi, T. Babut, E. Petit, M. Rolland, D. Quemener, L. Soussan, M. A. Moradi, M. Semsarilar, *Polym. Chem.* **2019**, *10*, 336.
[55] T. P. T. Dao, L. Vezenkov, G. Subra, M. Amblard, V. Ladmiral, M. Semsarilar, *Polym. Chem.* **2023**, *14*, 295.
[56] T. P. T. Dao, L. Vezenkov, G. Subra, V. Ladmiral, M. Semsarilar, *Polym. Chem.* **2021**, *12*, 113.
[57] A. Blanazs, R. Veber, O. O. Mykhaylyk, A. J. Ryan, J. Z. Heath, C. W. Ian Douglas, S. P. Armes, *J. Am. Chem. Soc.* **2012**, *134*, 9741.
[58] O. J. Dean, J. Jennings, S. P. Armes, *Chem. Sci.* **2021**, *12*, 13719.
[59] E. R. Jones, M. Semsarilar, P. Wyman, M. Boerakker, S. P. Armes, *Polym. Chem.* **2016**, *7*, 851.
[60] K. Matyjaszewski, J. Spanswick, *Mater. Today* **2005**, *8*, 26.
[61] E. E. Brotherton, F. L. Hatton, A. A. Cockram, M. J. Derry, A. Czajka, E. J. Cornel, P. D. Topham, O. O. Mykhaylyk, S. P. Armes, *J. Am. Chem. Soc.* **2019**, *141*, 13664.
[62] C. D. Spicer, C. Jumeaux, B. Gupta, M. M. Stevens, *Chem. Soc. Rev.* **2018**, *47*, 3574.
[63] E. Gazit, *Annu. Rev. Biochem.* **2018**, *87*, 533.